Journal of Materials Chemistry A

Accepted Manuscript

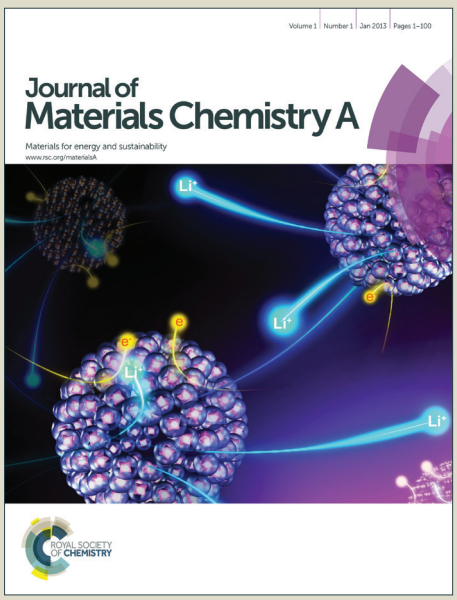

ROYAL SOCIETY OF CHEMISTRY

www.rsc.org/materialsA

Cite this: DOI: 10.1039/c0xx00000x

www.rsc.org/xxxxxx

ARTICLE TYPE

Hierarchical CNT@$NiCo_2O_4$ core-shell hybrid nanostructure for high performance supercapacitors

Feng Cai,[a, b] Yiran Kang,[a, c] Hongyuan Chen,[a] Minghai Chen,*[a] Qingwen Li,*[a]

Received (in XXX, XXX) Xth XXXXXXXXX 20XX, Accepted Xth XXXXXXXXX 20XX

DOI: 10.1039/b000000x

The mass integration of electrochemical active materials onto nanosized conductive fillers was a promising strategy to achieve an idea electrode structure for energy storage devices. In this research, one dimensional CNT@$NiCo_2O_4$ nanosheets core-shell structural nanocable was constructed by a facile chemical co-deposition route combined with post calcination in air. The subsequent thermal treatment led to the transformation of the hydroxide nanosheets precursor to $NiCo_2O_4$ nanosheets, during which process the overall morphology and structure were well retained. Selecting CNTs as conductive support for ultra-thin $NiCo_2O_4$ nanosheets, a high-performance electrode for supercapacitors was obtained. Notably, the as-prepared CNT@$NiCo_2O_4$ nanocables own a high capacitance of 1038 $F{\cdot}g^{-1}$ at a current density of 0.5 $A{\cdot}g^{-1}$. Furthermore, the specific capacitance of the product was almost 100% reserved after 1000 cycles, which indicates excellent structural and cycling stability. More importantly, a relatively high mass loading of active materials on CNTs was achieved as well, making the practical application of such electrode materials possible. Consequently, this CNTs@$NiCo_2O_4$ nanocable is a promising electrode for high performance supercapacitors.

1. Introduction

For the past few years, there has been an increasing demand of advanced energy storage systems for high power devices such as electric vehicles and mobile electronics. Supercapacitors (also called electrochemical capacitors) are attracting more and more attention from researchers worldwide,[1, 2] owing to their series of unique advantages (high power density, fast charge and discharge process, long cycle life and so on). Generally, electrode materials for supercapacitors can be divided into two categories based on the energy storage mechanism:[3, 4] electric double-layer capacitive materials (porous carbon materials) with large specific area and Faradaic capacitive materials (also called pseudocapacitive materials, including metallic oxide/hydroxide, conductive polymers, et al) fully taking advantages of fast and reversible redox reactions of the electrochemical active electrode materials.[5, 6] The former have excellent cyclic performance but poor specific capacitance for the limit of energy storage mechanism. While the latter showed ultra-high capacitance, but serves from their poor conductivity, which will make their practical capacitance much lower than theoretic value.

Transition metal oxides show ultra-high capacitance with other excellent performance such as green synthesis methods and low price.[7] Among metal oxides, spinel nickel cobaltite ($NiCo_2O_4$) is a very promising electrode material with ultra-high theoretic capacitance (higher than 3000 F/g) for supercapacitors. It is reported that nickel cobaltite shows many outstanding superiorities such as low cost, abundant resources and environmentally friendly.[8-10] In addition, nickel cobaltite exhibits a much better electrical conductivity, at least two orders of magnitude higher, and higher electrochemical activity when compared with nickel oxides and cobalt oxides.[11] These intriguing features make nickel cobaltite investigated widely and deeply. However, the low specific area of nickel cobaltite micrometer powder could largely reduce the contact area of the materials and electrolyte, which could largely decrease the practical capacitance of nickel cobaltite comparing with the theoretic value. Thus many reports focused on the preparation of nickel cobaltite nanostructure with large specific area and appropriate porous structure, such as nanoflowers,[12] aerogels,[11] and porous nanosheets/nanowires.[13, 14] However, the conductivity of nickel cobaltite is relatively poor for supercapacitors especially at large charge/discharge current densities. The integration of nickel cobaltite nanostructure with conductive fillers could solve this problem in a certain extend.[8, 15-18]

CNTs are gradually regarded as promising candidates for high-performance electrodes owing to their excellent conductivity, high specific surface area, very high strength, chemical stability and low density.[19-21] So far, various of active materials, like PANI,[22] CuS nanoneedles,[23] Ni_3S_2 Nanosheets,[24] TiO_2,[25] SnO_2[26], have been grown on one-dimensional CNTs. Although there are several works focused on CNTs supported $NiCo_2O_4$ have been reported,[15, 27-29] it is still a challenge for the directly large-mass growth of $NiCo_2O_4$ nanostructure on carbon nanotubes by a facile mean. In this work, we controllably grew $NiCo_2O_4$ nanosheets on individual CNTs via a simple chemical bath deposition (CBD) method at room temperature followed by a post annealing treatment. The introduction of CNTs brought great benefit to the

conductivity increase and surface area per mass ratio of $NiCo_2O_4$. In addition, lightweight but free-standing CNTs are strong enough to be covered by $NiCo_2O_4$ nanosheets, that is, a relatively large mass loading of nickel cobaltite on CNTs is easily gained. As a result, the CNT@$NiCo_2O_4$ nanosheets hybrid exhibits an ultrahigh specific capacitance and excellent cycling stability.

2. Experimental Section

Materials. All the reagents used were of analytical grade and used without further purification. $NiCl_2{\cdot}6H_2O$, Polyvinylpyrrolidone (PVP) and $NH_3{\cdot}H_2O$ (25-28 wt %) were obtained from Sino Pharm Chemical Reagent. $CoCl_2{\cdot}6H_2O$ was purchased from Aladdin Chemistry Co, Ltd. Multi-walled carbon nanotube was prepared by floating catalyst chemical vapor deposition (FCCVD) method. The absolute ethanol was purchased from Chinasun Specialty Products Co, Ltd.

Synthesis. In a typical procedure, 35 mg MWCNT powder was mixed with 7 $mg{\cdot}ml^{-1}$ PVP aqueous solution. After the MWCNT was uniformly dispersed with the assistance of ultrasonication under 400 W for 0.5 h, the resultant solution was mixed with 0.004 mol $CoCl_2{\cdot}6H_2O$ and 0.002 mol $NiCl_2{\cdot}6H_2O$. Then the solution was stirred for half an hour at room temperature to form a black solution, followed by the drop by drop addition of 5% $NH_3{\cdot}H_2O$ solution until its pH reached 9. Being kept still for 3 h, the obtained precipitate was filtered, washed with water and ethanol several times to remove the surfactant and the residual ions, and dried at 70 ^oC for 12 h under vacuum. Finally, the hybrid precursor was annealed in air at 300 ^oC for 3 h with a slow heating rate of 1 $^oC{\cdot}min^{-1}$ in order to obtain CNT@$NiCo_2O_4$ nanostructure. For comparison, the pure $NiCo_2O_4$ powder was also prepared under the same condition but without the addition of CNT dispersion.

Materials Characterization. The samples were characterized by field-emission scanning electron microscopy (FESEM, Quanta 400FEG, FEI), X-ray Energy Dispersive Spectrometer (EDS, Apollo40SDD) and Transmission electron microscope (TEM, Tecnai G2 F20 S-Twin, FEI). The structure of the products was examined by X-ray powder diffraction (XRD, D8Advance, Bruker AXS). The BET specific surface area and the pore size distribution of the sample were investigated by the Brunauer-Emmett-Teller (BET) and the Barrett-Joyner-Halenda (BJH) method. Thermogravimetric analysis(TGA, SDT 2960， DSC 2010) was used to estimate the mass content of the $NiCo_2O_4$ nanosheets in the CNT@$NiCo_2O_4$ hybrid.

Electrochemical Measurements. The working electrodes were prepared by pressing the as-prepared samples directly onto nickel foam current collector. Electrochemical measurements (CHI 660D electrochemical workstation) were conducted in a three-electrode configuration at room temperature using 6 M KOH as electrolyte, a platinum wire as the counter electrode, a saturated calomel electrode(SCE) as the reference electrode, respectively. Electrochemical impedance spectroscopy (EIS) measurements were carried out by applying an AC voltage with 5 mV amplitude in a frequency range from 0.01 Hz to 100 kHz at open circuit potential. Cycling stability measurement of the sample was carried out on a Land battery testing system.

3. Results and discussion

Fig. 1 shows XRD patterns of CNT@$NiCo_2O_4$ precursor (hydroxide) and CNT@$NiCo_2O_4$ powder. The CNT@$NiCo_2O_4$ precursor shares the same crystalline structure with hydrous α-$Ni(OH)_2$ (JCPDF card no. 22-0444).[30]

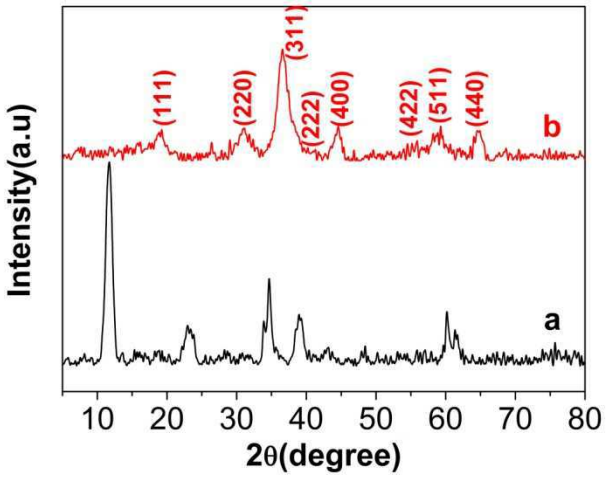

Fig. 1 A reprensentive wide-angle XRD patterns of CNT@$NiCo_2O_4$ precursor (a) and CNT@$NiCo_2O_4$ powder (b).

As shown in Fig. 1b, eight characteristic diffraction peaks appeared can be readily indexed to the planes of cubic $NiCo_2O_4$ phase (JCPDF card no. 20-0781). It is worthy to mention that no other peaks are shown, which effectively confirms the purity of the obtained $NiCo_2O_4$ phase that was supported on one-dimensional CNTs. In other words, the conditions we chose to transform the CNT@$NiCo_2O_4$ precursor to CNT@$NiCo_2O_4$ are proper.

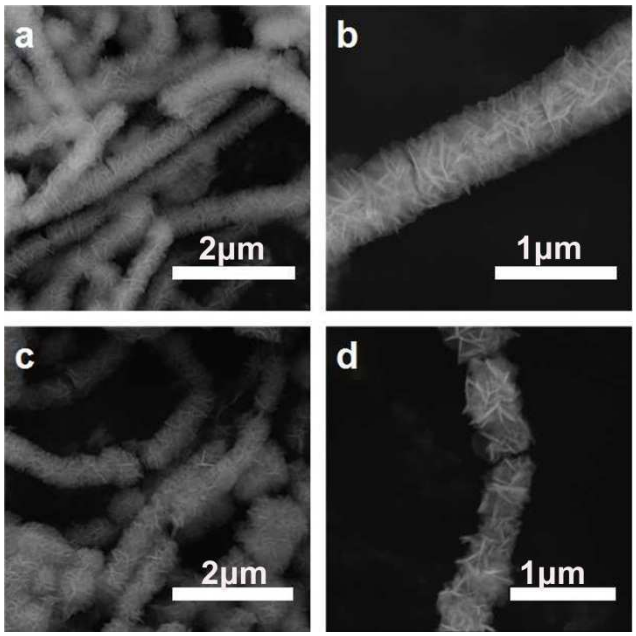

Fig. 2 Typical FESEM images of CNT@$NiCo_2O_4$ precursor (a, b) and CNT@$NiCo_2O_4$ nanostructure annealed at 300 ^oC for 3 h in the air (c, d).

SEM images of CNT@$NiCo_2O_4$ precursor and CNT@$NiCo_2O_4$ are presented in Fig. 2. Fig. 2a and b indicate FESEM images of CNT@$Ni_{0.33}Co_{0.67}(OH)_2$. As can be seen, numerous hydroxide

nanosheets were found well grown around individual CNTs to form a conformal coating on the surface. From the enlarged view (Figure. 2b), the nanosheets are in mutual contact, which might own better mechanical strength and form a better conductive network not be easily detached from CNT core. Such nanostructure may bring much benefit to the increase of its specific area while keep a conductive core, which is of great importance to electrochemical performance of electrode materials.[7] From Fig. 2c and d, we can see that the morphology of the composite nanocables did not change after Ni-Co hydroxide being converted into $NiCo_2O_4$. Evidently, few $NiCo_2O_4$ nanosheets tend to be agglomerated.

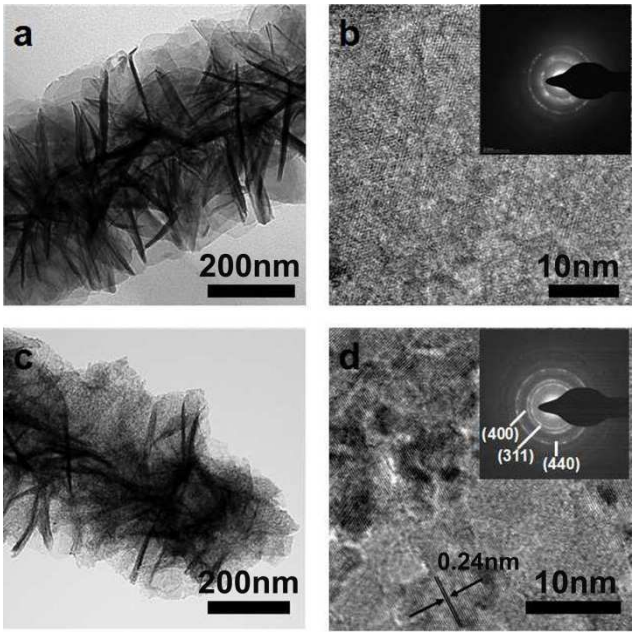

Fig. 3 Typical TEM images of CNT@$NiCo_2O_4$ precursor (a, b) and CNT@$NiCo_2O_4$ nanostructure annealed at 300 °C for 3 h in the air (c, d).

As shown in Fig. 3, TEM and selected area electron diffraction are used to further study the crystallographic properties of the obtained CNT@Ni-Co hydroxide and CNT@$NiCo_2O_4$. Fig. 3a and b show the corresponding TEM images of the CNT@Ni-Co hydroxide. The ultra-thin hydroxide nanosheets exhibit flower-like morphology. Compared with CNT@$NiCo_2O_4$, the hydroxide owes a larger interplane spacing, which is aroused by the existence of the water molecule in the crystalline structure. The SAED pattern, which has been taken from a selected area of nanosheets, indicates the polycrystalline characteristic of the nanosheets. As can be seen in the TEM images of the CNT@ $NiCo_2O_4$ (Fig. 3c), the thin oxide nanosheets are highly porous, consisted of nanocrystallites with the size around 10–15 nm, which results from the thermal decomposition of the hydroxides.[14] The high resolution TEM (HRTEM) examination shown in Fig. 3d reveals a distinct set of visible lattice fringes with an inter-planar spacing of 0.24 nm, which is corresponding to the (311) plane of spinel $NiCo_2O_4$. The polycrystalline structure of $NiCo_2O_4$ nanosheets is demonstrated by the SAED pattern, which shows well-defined rings. Specifically, these rings can be indexed to (311), (400), (440) planes of $NiCo_2O_4$, which one step further confirms the XRD characterization. The results above show that CNTs are well suitable substrates for spinel nickel cobaltite's nucleation and crystal growth. Furthermore, the interspace between $NiCo_2O_4$ nanosheets become larger compared with the sample without annealing treatment. The unique features mentioned above can make CNT@$NiCo_2O_4$ hybrid nanostructure accessible to electrolytes in a larger extent, which makes the nanostructure a potential candidate as electrodes for supercapacitors with high specific capacitance and excellent cycling stability. [31]

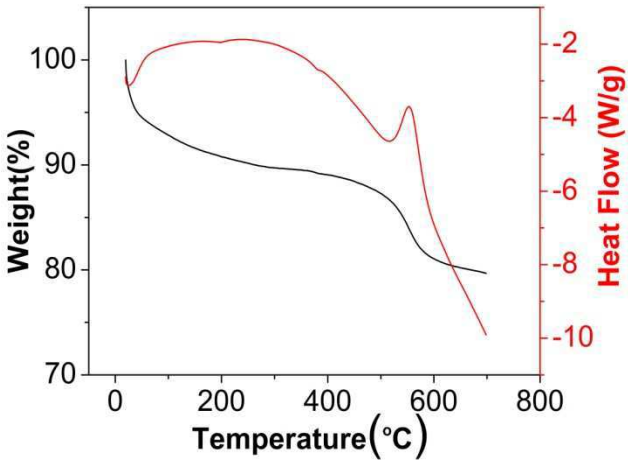

Fig. 4 TGA-DSC measurement of CNT@$NiCo_2O_4$ nanostructure in the air with a temperature rate of 10 $K \cdot min^{-1}$.

For the purpose of evaluating the content of $NiCo_2O_4$ in this CNT@$NiCo_2O_4$ composite nanostructure, TGA was used. As seen from Fig. 4, the mass ratio of $NiCo_2O_4$ in the hybrid is roughly 80%.

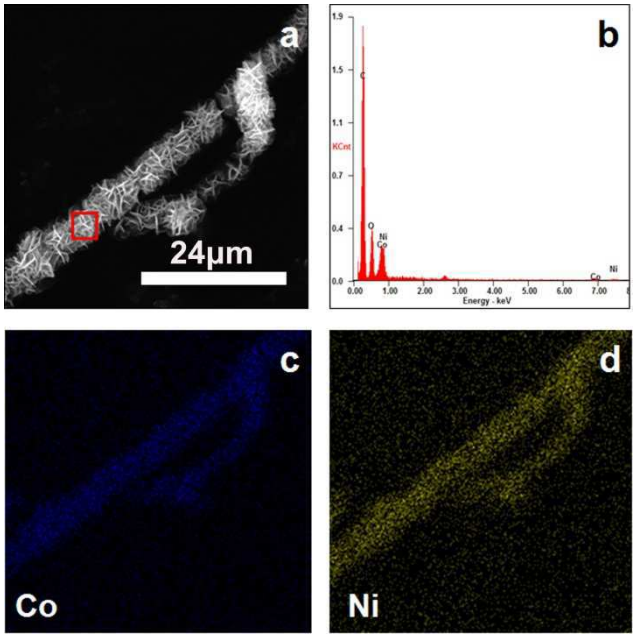

Fig. 5 EDS test (a, b) and mapping (c, d) of CNT@$NiCo_2O_4$ nanostructure, respectively.

The EDS measurement (Fig. 5a, b) shows that the molar ratio of Ni to Co is almost 1:2, which is in accordance with the result

of XRD. Line EDS mapping technique was conducted used to examine Co/Ni element distribution in the composite nanocable. The result shows a uniform distribution of the two elements, which could be used to confirm the single phase of $NiCo_2O_4$ and its good coverage around CNTs (see Fig. 5c and d).

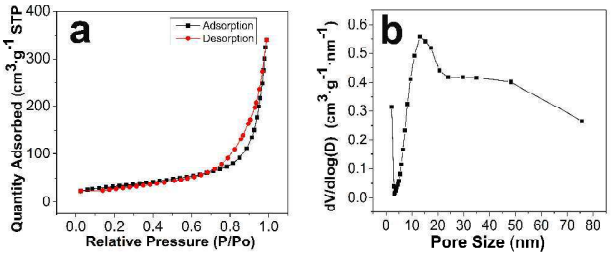

Fig. 6 N_2 adsorption-desorption isotherm of CNT@$NiCo_2O_4$ nanostructure (a); BJH measurement of CNT@$NiCo_2O_4$ nanostructure (b).

In addition, the porous characteristics of the sample mentioned above was further studied by nitrogen adsorption and desorption measurement, as presented in Fig. 6. Fig.6a shows adsorption-desorption isotherm of CNT@$NiCo_2O_4$ hybrid nanocables. It's a typical III-type isotherm, which could be attributed to N_2 adsorption-desorption in metallic oxide structures. The calculated specific surface area of the hybrid nanocables is 115 $m^2 \cdot g^{-1}$ according to BET test. The large specific area could largely increase the utilization of $NiCo_2O_4$ as an electrochemical active material in electrodes.[32] Fig. 6b shows the corresponding pore size distribution calculated by the BJH model. As can be seen, the product possesses a wide pore size distribution, which is attributed to the mesoporous structure of $NiCo_2O_4$ nanosheets and the large pore between these nanosheets. This hierarchically porous structure facilitates the mass transportation of electrolytes within in the bulk of electrode materials, promoting electrolyte accessibility, kinetic reversibility, and electrochemical reaction homogeneity.[33, 34]

The electrochemical performance of CNT@$NiCo_2O_4$ hybrid nanocables was investigated in a three-electrode system. The results are shown in Fig.7. Fig. 7a shows the representative cyclic voltammetry curves of CNT@$NiCo_2O_4$ hybrid nanocable electrode at different scan rates ranging from 1 $mv \cdot s^{-1}$ to 50 $mv \cdot s^{-1}$. Clearly, a pair of redox peaks can be observed in these CV curves, which should be attributed to the Faradaic redox reactions related to M-O/M-O-O-H (M represents Ni and Co ions).[35, 36] Fig.7b shows a CV curve comparison of the hybrid nanocables and pure $NiCo_2O_4$ nanoflower powder at a scan rate of 5 $mV \cdot s^{-1}$. The results show that the basic features of the CV curve for pure $NiCo_2O_4$ powder almostly keeps the same as the sample of CNT@$NiCo_2O_4$ hybrid nanocables, while the area covered by CV curve of CNT@$NiCo_2O_4$ hybrid nanocables is larger compared with the former, which indicates that the capacitance calculated from the CV curves is higher.[16] Fig. 7c shows galvanostatic charge/discharge plots of the sample within a potential range of -0.1 to 0.36 V at various current densities ranging from 0.5 $A \cdot g^{-1}$ to 10 $A \cdot g^{-1}$. It is noted that the potential-time curves at all current densities are nearly symmetric, in other words, the electrode exhibits outstanding charge-discharge with a stable coulombic efficiency, low polarization as well.[37] Based on the charge-discharge curves, the specific capacitance of CNT@$NiCo_2O_4$ hybrid nanocables can be calculated by the formula ($C = I\Delta t/m\Delta V$,

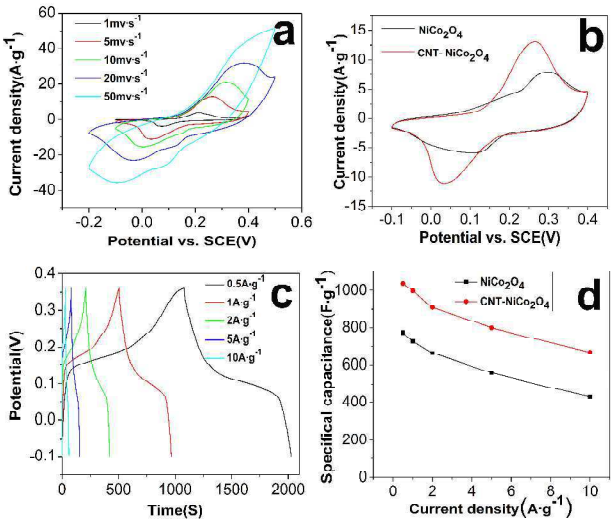

Fig. 7 CV curves of CNT@$NiCo_2O_4$ at different scan rate (a); CV curves of pure $NiCo_2O_4$ and CNT@$NiCo_2O_4$ powder separately at 5 $mv \cdot s^{-1}$ (b); Charge and discharge profiles of CNT@$NiCo_2O_4$ at various current densities (c); the rate performance (d).

where I is the discharge current, Δt is the discharge time, ΔV is the sweeping voltage range, m is the total mass of the electrode material.[38] The calculated rate performance of the hybrid cables is shown in Fig. 7d. It can be observed that the specific capacitance can achieve a maximum of 1038 $F \cdot g^{-1}$ at a current density of 0.5 $A \cdot g^{-1}$. Even at a current density as high as 10 $A \cdot g^{-1}$, 667 $F \cdot g^{-1}$ can still be retained, which suggests that about 36% of the specific capacitance is lost when the current density increases from 0.5 $A \cdot g^{-1}$ to 10 $A \cdot g^{-1}$. For comparison, the pure $NiCo_2O_4$ nanoflower powder shows a lower capacitance and poorer rate performance in the same condition (as shown in Fig.7d). The capacitance of the powder decreases from 775 $F \cdot g^{-1}$ (at 0.5 $A \cdot g^{-1}$) to 430 $F \cdot g^{-1}$ (at 10 $A \cdot g^{-1}$), with a reduction of 45%. It easily comes to the conclusion that the rate capacitance of CNT@$NiCo_2O_4$ is superior to that of pure $NiCo_2O_4$. The good superior electrochemical performance of CNT@$NiCo_2O_4$ should be attributed to good conductive performance of the nanocable with a highly conductive CNT core.

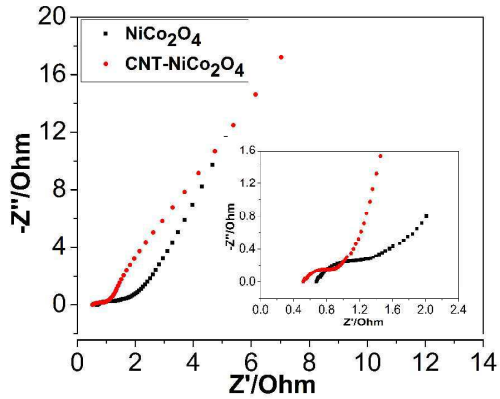

Fig. 8 Niquist plots of CNT@$NiCo_2O_4$.

Nyquist plots of the EIS spectra of $NiCo_2O_4$ powder and CNT@$NiCo_2O_4$ are shown in the Fig. 8. From the intercepts of the high frequency semicircle with the real axis at R_s and (R_s+R_{ct}), the bulk solution resistance R_s and charge-transfer resistance R_{ct} can be calculated.[32] According to the data, the solution resistance R_s and R_{ct} of the CNT@$NiCo_2O_4$ hybrid nanocables are 0.517 Ω and 0.483 Ω, respectively. In contrast to the CNT@$NiCo_2O_4$, the bulk solution resistance R_s and the charge transfer resistance R_{ct} of $NiCo_2O_4$ have a higher value of 0.675 Ω and 0.849 Ω, separately. Notably, the charge transfer resistance R_{ct}, also called Faraday resistance, is a factor that impact on the specific power of a supercapacitor.[39, 40] That is to say, the lower charge transfer resistance R_{ct} of CNT@$NiCo_2O_4$ could endow the electrode with a high power density.

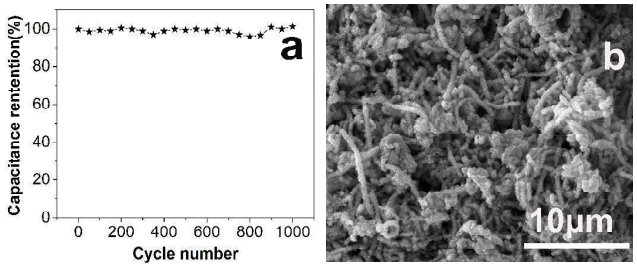

Fig. 9 The cycling performance of CNT@$NiCo_2O_4$ at a current density of 2 $A{\cdot}g^{-1}$ (a); the FESEM image of the CNT@$NiCo_2O_4$ sample after electrochemical measurement (b).

Fig. 9a shows the cyclic performance of CNT@$NiCo_2O_4$ hybrid nanocables at a current density of 2 $A{\cdot}g^{-1}$. It can be observed that the specific capacitance of the sample keeps stable with almost 100% of the original value during 1000 cycles of charge/discharge. Furthermore, SEM image (Fig. 9b) of the sample hybrid nanocables after cyclic measurement shows that $NiCo_2O_4$ nanosheets are still kept on CNT cores with their original structure, which demonstrates the structural stability of these nanocables as the electrode for supercapacitors.

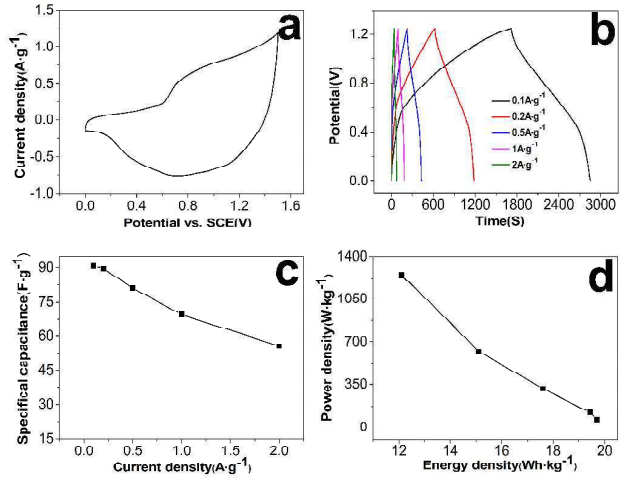

Fig. 10 CV profile of the fabricated asymmetric supercapacitor at 5 $mv{\cdot}s^{-1}$ (a); Charge and discharge profiles of the fabricated asymmetric supercapacitor at various current densities (b); the rate performance (c) and Ragone plot (d) of the asymmetric supercapacitor.

To further evaluate the CNT@$NiCo_2O_4$ composite for real device application, we fabricated asymmetric capacitors in our home-made two-electrode test system using CNT@$NiCo_2O_4$ hybrid nanocables and commercially available activated carbon as positive and negative electrodes respectively with mass ratio of 2:5. The results of electrochemical test of the asymmetric capacitors are presented in Fig. 10. Fig. 10a shows a CV curve of the asymmetric capacitors at a scan rate of 5 $mV{\cdot}s^{-1}$, whose shape is relatively full. To further evaluate the performance of the cell, galvanostatic charge–discharge testing was measured at various current densities(Fig. 10b). The calculated specific capacitance of the asymmetric capacitor is 91 $F{\cdot}g^{-1}$ at a current density of 0.5 $A{\cdot}g^{-1}$, and 56 $F{\cdot}g^{-1}$ at 2 $A{\cdot}g^{-1}$ as shown in Fig. 10c. Ragone plot (see Fig. 10d) calculated from charge/discharge curves illustrates power density against energy density for the fabricated asymmetric supercapacitor. Working in a potential range of 1.25 V, the supercapacitor exhibits a relatively high energy density of 19.7 $Wh{\cdot}kg^{-1}$ at a power density of 62.5 $W{\cdot}kg^{-1}$ and an energy density of 12.1 $Wh{\cdot}kg^{-1}$ can still be kept even at a power density of 1250 $W{\cdot}kg^{-1}$, which may be one of the choices for a variety of emerging energy applications.

These results mentioned above clearly confirm that the CNT@$NiCo_2O_4$ hybrid nanocables own excellent electrochemical performance with good rate performance and high power/energy density, which could be derived from the factors as follows. Firstly, using nanosized conductive support such as CNTs, $NiCo_2O_4$ can be dispersed over a large area, effectively keeping itself from further growth by agglomeration and making sure that the active electrode materials are fully utilized. As a result, in addition to providing double-layer capacitance, the introduction of CNT boosts the specific surface area of the hybrid and improves the contact between electrode and electrolyte. Secondly, CNTs, has superior conductive performance and good mechanical property with excellent environmental stability. These individual CNT cores could form a three-dimensional conductive network in the electrode, contributing to the improvement of the electrode's electrical conductivity and facilitating the transportation of electron and ion within the bulk electrode material.

4. Conclusions

In this work, we have developed a facile CBD method coupled with a post annealing treatment to grow ultra-thin spinel $NiCo_2O_4$ nanosheets with large mass on individual CNTs. These ultra-thin nanosheets with porous nanostructure could be firmly fixed with CNT backbone even after long charge/discharge cyclic test. This hybrid structure could achieve both high conductive performance and large specific area as the electrode for supercapacitors. The synergistic effect, aroused from the integration of CNTs and the ultra-thin $NiCo_2O_4$ nanosheets, endows the CNT@$NiCo_2O_4$ hybrid nanostructure with high capacitance and excellent cyclic stability as the electrode materials for supercapacitors. When measured at the current density of 0.5 $A{\cdot}g^{-1}$, the CNT@$NiCo_2O_4$ sample shows a high capacitance of 1038 $F{\cdot}g^{-1}$. Furthermore, it is intriguing to note that the specific capacitance of the hybrid structure keeps stable during 1000 cycles of charge/discharge test at a current density of 2 $A{\cdot}g^{-1}$. These excellent performances make this hybrid nanocable a promising candidate as the electrode materials for high performance supercapacitors.

Acknowledgement

The project was supported by the National Science Foundation of China (No.21203238), the National Basic Research Program (No.2010CB934700), and Production and Research Collaborative Innovation Project of Jiangsu Province, China (No. BY2011178).

Notes and references

[a]*Suzhou Institute of Nano-tech and Nano-bionics, Chinese Academy of Sciences, Suzhou 215123, P. R. China; Tel: 0512-62872803; E-mail: mhchen2008@sinano.ac.cn*
[b]*School of Nano Science and Technology, University of Science and Technology of China, Suzhou, 215123, P. R. China;*
[c]*School of Materials Science and Engineering, Zhengzhou University, Zhengzhou, 450001, P. R. China.*

1. P. Simon and Y. Gogotsi, Nature materials, 2008, 7, 845-854.
2. J. R. Miller and P. Simon, Science Magazine, 2008, 321, 651-652.
3. G. Wang, L. Zhang and J. Zhang, Chemical Society reviews, 2012, 41, 797-828.
4. B. Conway, Electrochemical supercapacitors: scientific fundamentals and technological applications (POD), Kluwer Academic/Plenum: New York, 1999.
5. L. L. Zhang and X. S. Zhao, Chemical Society reviews, 2009, 38, 2520-2531.
6. H. Jiang, J. Ma and C. Li, Advanced materials, 2012, 24, 4197-4202.
7. M. Zhi, C. Xiang, J. Li, M. Li and N. Wu, Nanoscale, 2013, 5, 72-88.
8. H.-W. Wang, Z.-A. Hu, Y.-Q. Chang, Y.-L. Chen, H.-Y. Wu, Z.-Y. Zhang and Y.-Y. Yang, Journal of Materials Chemistry, 2011, 21, 10504.
9. A. C. Tavares, M. A. M. Cartaxo, M. I. da Silva Pereira and F. M. Costa, J Solid State Electrochem, 2001, 5, 57-67.
10. H. Jiang, J. Ma and C. Li, Chemical communications, 2012, 48, 4465.
11. T. Y. Wei, C. H. Chen, H. C. Chien, S. Y. Lu and C. C. Hu, Advanced materials, 2010, 22, 347-351.
12. Z.-Q. Liu, K. Xiao, Q.-Z. Xu, N. Li, Y.-Z. Su, H.-J. Wang and S. Chen, RSC Advances, 2013, 3, 4372.
13. L. Yu, G. Zhang, C. Yuan and X. W. Lou, Chemical communications, 2013, 49, 137-139.
14. C. Yuan, J. Li, L. Hou, X. Zhang, L. Shen and X. W. D. Lou, Advanced Functional Materials, 2012, 22, 4592-4597.
15. X. Wang, X. Han, M. Lim, N. Singh, C. L. Gan, M. Jan and P. S. Lee, Journal of Physical Chemistry C, 2012, 116, 12448-12454.
16. H. Wang, C. M. B. Holt, Z. Li, X. Tan, B. S. Amirkhiz, Z. Xu, B. C. Olsen, T. Stephenson and D. Mitlin, Nano Research, 2012, 5, 605-617.
17. J. Du, G. Zhou, H. Zhang, C. Cheng, J. Ma, W. Wei, L. Chen and T. Wang, ACS applied materials & interfaces, 2013.
18. X. Wang, W. S. Liu, X. Lu and P. S. Lee, Journal of Materials Chemistry, 2012, 22, 23114.
19. J. M. Schnorr and T. M. Swager, Chemistry of Materials, 2010, 23, 646-657.
20. I. Dumitrescu, P. R. Unwin and J. V. Macpherson, Chemical communications, 2009, 6886-6901.
21. X. Chen, H. Zhu, Y.-C. Chen, Y. Shang, A. Cao, L. Hu and G. W. Rubloff, ACS Nano, 2012, 6, 7948-7955.
22. X. Zhang, J. Zhang, R. Wang and Z. Liu, Carbon, 2004, 42, 1455-1461.
23. T. Zhu, B. Xia, L. Zhou and X. W. D. Lou, Journal of Materials Chemistry, 2012, 22, 7851-7855.
24. T. Zhu, H. B. Wu, Y. Wang, R. Xu and X. W. D. Lou, Advanced Energy Materials, 2012, 2, 1497-1502.
25. F.-F. Cao, Y.-G. Guo, S.-F. Zheng, X.-L. Wu, L.-Y. Jiang, R.-R. Bi, L.-J. Wan and J. Maier, Chemistry of Materials, 2010, 22, 1908-1914.
26. G. Chen, Z. Wang and D. Xia, Chemistry of Materials, 2008, 20, 6951-6956.
27. F. Deng, L. Yu, G. Cheng, T. Lin, M. Sun, F. Ye and Y. Li, Journal of Power Sources, 2014, 251, 202-207.
28. G. Zhang and X. W. David Lou, Scientific reports, 2013, 3, 1470.
29. W.-w. Liu, C. Lu, K. Liang and B. K. Tay, Journal of Materials Chemistry A, 2014, 2, 5100-5107.
30. G.-W. Yang, C.-L. Xu and H.-L. Li, Chemical communications, 2008, 6537-6539.
31. Y. Hou, Y. Cheng, T. Hobson and J. Liu, Nano letters, 2010, 10, 2727-2733.
32. P. G. Bruce, B. Scrosati and J. M. Tarascon, Angewandte Chemie, 2008, 47, 2930-2946.
33. R.-T. Wang, L.-B. Kong, J.-W. Lang, X.-W. Wang, S.-Q. Fan, Y.-C. Luo and L. Kang, Journal of Power Sources, 2012, 217, 358-363.
34. G. Zhang and X. W. Lou, Advanced materials, 2013, 25, 976-979.
35. H. Wang, Q. Gao and L. Jiang, Small, 2011.
36. C. Yuan, X. Zhang, L. Su, B. Gao and L. Shen, Journal of Materials Chemistry, 2009, 19, 5772-5777.
37. W.-M. Zhang, X.-L. Wu, J.-S. Hu, Y.-G. Guo and L.-J. Wan, Advanced Functional Materials, 2008, 18, 3941-3946.
38. H. B. Li, M. H. Yu, F. X. Wang, P. Liu, Y. Liang, J. Xiao, C. X. Wang, Y. X. Tong and G. W. Yang, Nature communications, 2013, 4, 1894.
39. J. Zang, S.-J. Bao, C. M. Li, H. Bian, X. Cui, Q. Bao, C. Q. Sun, J. Guo and K. Lian, The Journal of Physical Chemistry C, 2008, 112, 14843-14847.
40. L. Bao, J. Zang and X. Li, Nano letters, 2011, 11, 1215-1220.

Graphical Abstract

Ultrathin $NiCo_2O_4$ nanosheets directly grown on one dimensional CNTs as high performance electrode materials for supercapacitors were synthesized through a facile chemical co-deposition process combined with post calcination in air.